Journal of Alloys and Compounds 509 (2011) 332–337

Contents lists available at ScienceDirect

Journal of Alloys and Compounds

journal homepage: www.elsevier.com/locate/jallcom

Synthesis and photoluminescence of a novel Sr-SiAlON:Eu^{2+} blue-green phosphor ($Sr_{14}Si_{68-s}Al_{6+s}O_sN_{106-s}$:$Eu^{2+}$ ($s \approx 7$))

Kousuke Shioi [a,*], Yuichi Michiue [b], Naoto Hirosaki [b], Rong-Jun Xie [b], Takashi Takeda [b], Yoshitaka Matsushita [c], Masahiko Tanaka [c], Yuan Qiang Li [b]

[a] Showa Denko K.K., R and D Centre, Ohnodai, Midori, Chiba 267-0056, Japan
[b] National Institute for Materials Science, Tsukuba, Ibaraki 305-0044, Japan
[c] National Institute for Materials Science, SPring-8, Sayo, Hyogo 679-5148, Japan

ARTICLE INFO

Article history:
Received 16 March 2010
Received in revised form 2 September 2010
Accepted 3 September 2010
Available online 16 September 2010

Keywords:
SiAlON
Nitride
Phosphor
Structure
Luminescence

ABSTRACT

A novel Eu^{2+} activated Sr-SiAlON oxynitride phosphor, with the chemical composition of $Sr_{14}Si_{68-s}Al_{6+s}O_sN_{106-s}$:$Eu^{2+}$ ($s \approx 7$), was synthesized by firing the powder mixture of SrO, $SrSi_2$, α-Si_3N_4, AlN and Eu_2O_3 at 1900 °C for 6 h under 1 MPa nitrogen atmosphere. The structure has a typical feature of SiAlON consisting of the host framework which is constructed by a three-dimensional MX_4 tetrahedral (M: Si or Al; X: O or N) network, and Sr or Eu^{2+} ions as the guest ions. It has been shown that the Sr-SiAlON:Eu^{2+} phosphor has the excitation band covering the range of the ultraviolet light region to 500 nm, and exhibits an intense blue-green color with the emission band centered at about 508 nm. The temperature dependent emission intensity of the Sr-SiAlON:Eu^{2+} phosphor is better than that of a typical blue-green Ba_2SiO_4:Eu^{2+} phosphor. It is demonstrated that Sr-SiAlON:Eu^{2+} phosphor is very promising for use in white -LEDs.

1. Introduction

White light-emitting diodes (white-LEDs) are considered as next generation solid state lighting systems because of their excellent properties such as low power consumption, high efficiency, long lifetime, and free of toxic mercury. The availability of white-LEDs should open up a great number of new exciting application fields: white light sources to replace traditional incandescent and fluorescent lamps, backlights for portable electronics, automobile headlights, medical, and architecture lighting, etc. [1–4].

Rare-earth-doped oxynitride or nitride luminescent materials have become the most important wavelength-conversion phosphors for use in white-LEDs embedded on (In, Ga)N chips due to their strong absorption and high conversion efficiency in the near-UV and blue spectral range. Typical examples are red-emitting $M_2Si_5N_8$:Eu^{2+} (M = Ca, Sr, and Ba) [5,6], $CaAlSiN_3$:Eu^{2+} [7,8], $Sr_xCa_{1-x}AlSiN_3$:Eu^{2+} [9], orange-red $SrSiAl_4N_7$:Eu^{2+} [10], yellow-emitting Ca-α-SiAlON:Eu^{2+} [11–14], $Ba_2AlSi_5N_9$:Eu^{2+} [15] and Ce-melilite [16], green-emitting β-SiAlON:Eu^{2+} [17], and blue emitting $BaSi_7N_{10}$:Eu^{2+} [18], $BaSi_6N_8O$:Eu^{2+} [19], and α-Si_3N_4:Eu^{2+} [20]. Among these (oxy)nitride luminescence materials, β-SiAlON:Eu^{2+} phosphor has a strong absorption in the range of UV to blue region and exhibits a green emission with the peak wavelength at 535 nm [17]. Additionally, blue-green emitting phosphors with shorter peak wavelength than that of β-SiAlON:Eu^{2+} phosphor are required to realize high color rendering index in the case of lighting and wide color gamut in the case of display. Ba_2SiO_4:Eu^{2+} is well known as a blue-green phosphor with the peak wavelength of 505 nm [21]. However, the emission intensity of Ba_2SiO_4:Eu^{2+} phosphor decreases significantly at high temperature because of thermal quenching [22].

Recently, novel green or blue-green emitting Eu^{2+} activated Sr-SiAlON phosphors have been developed. Fukuda et al. reported $Sr_3Si_{13}Al_3O_2N_{21}$:Eu^{2+} phosphor with the emission peak wavelength ranging from 515 to 525 nm [23]. Subsequently, Ishizawa et al. presented the crystal structure of $Sr_3Si_{15-x}Al_{1+x}O_xN_{23-x}$:$Eu^{2+}$ ($x \approx 2$), which is similar to $Sr_3Si_{13}Al_3O_2N_{21}$:Eu^{2+} [24]. Further, the $Sr_5Si_{21-x}Al_{5+x}O_{2+x}N_{35-x}$:$Eu^{2+}$ ($x \approx 0$) phosphor with the emission spectrum peaking at about 510 nm was synthesized [25]. Additionally, we reported the crystal structure of $Eu_3Si_{15-x}Al_{1+x}O_xN_{23-x}$ ($x \approx 5/3$) [26], which is basically isotypic to $Sr_3Si_{15-x}Al_{1+x}O_xN_{23-x}$:$Eu^{2+}$ ($x \approx 2$) [24]. From the viewpoint of higher-dimensional crystallography [27,28] which was originally developed for the analysis of incommensurate structures [29–31], both of $A_3Si_{15-x}Al_{1+x}O_xN_{23-x}$ (A: Sr^{2+} or Eu^{2+}) and $Sr_5Si_{21-x}Al_{5+x}O_{2+x}N_{35-x}$:$Eu^{2+}$ ($x \approx 0$) are considered as commensurate phases belonging to a series of compositely modulated structures, that is so-called composite crystals. A unified structure

* Corresponding author. Tel.: +81 29 851 3354x8865; fax: +81 29 851 3613.
E-mail address: SHIOI.Kousuke@nims.go.jp (K. Shioi).

0925-8388/$ – see front matter © 2010 Elsevier B.V. All rights reserved.
doi:10.1016/j.jallcom.2010.09.021

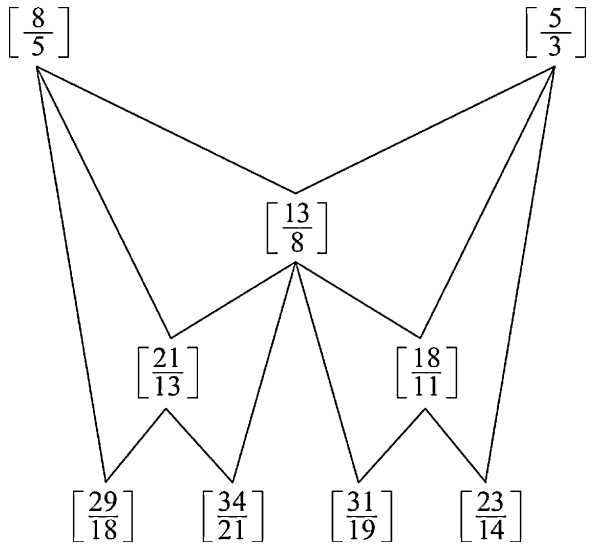

Fig. 1. Scheme of the Farey tree within the interval of [8/5, 5/3]. A phase $[n/m]$ is defined from the two generators indicated by solid lines, $[n_1/m_1]$ and $[n_2/m_2]$, as $[n/m] = [(n_1 + n_2)/(m_1 + m_2)]$.

model in (3+1)-dimensional superspace was proposed [26], from which the two structures are derived despite different crystal systems and space groups. The composite crystal model consists of two substructures with different periodicities along the *a*-axis. The chemical composition is AM_2X (M: Si or Al, X: O or N) for the 1st substructure and M_2X_4 for the 2nd substructure. For a phase in which the ratio of dimensions for the *a*-axis in the two substructures is $a_1/a_2 = n/m$, the chemical composition of a whole crystal is generally given by $(AM_2X)_m(M_2X_4)_n$. A phase of $a_1/a_2 = n/m$ is represented by $[n/m]$, hereafter. $A_3Si_{15-x}Al_{1+x}O_xN_{23-x}$ and $Sr_5Si_{21-x}Al_{5+x}O_{2+x}N_{35-x}$ are represented by [5/3] and [8/5], respectively. Consequently, other $[n/m]$ phases, which have been systematically given by the so-called Farey tree (Fig. 1), are expected to form [26]. In this study, a new Sr-SiAlON:Eu^{2+} phosphor was identified as one of the predicted phases in the composite crystal series other than [5/3] and [8/5], and then the photoluminescence spectrum of the newly obtained Sr-SiAlON:Eu^{2+} phosphor was reported and compared with that of [5/3]. Finally, the thermal stability of this new phosphor was investigated.

2. Experimental

A new Sr-SiAlON:Eu^{2+} phosphor other than [5/3] and [8/5] was prepared from the mixture of α-Si_3N_4 (SN-E10, Ube Industries Ltd., Japan), SrO (Kojyundo Chemical Laboratotry Co. Ltd., Japan), $SrSi_2$ (Kojyundo Chemical Laboratory Co. Ltd., Japan), AlN (Type F, Tokuyama Co. Ltd., Japan), and Eu_2O_3 (Shin-Etsu Chemical Co. Ltd., Japan). The starting composition of $Sr_{13.72}Eu_{0.28}Si_{60.2}Al_{12.32}O_{4.2}N_{99.4}$ was prepared from α-Si_3N_4: 33.84 mol %, SrO: 9.80 mol %, $SrSi_2$: 24.50 mol %, AlN: 31.51 mol %, and Eu_2O_3: 0.35 mol % (composition #1). $SrSi_2$ was used as the Sr^{2+} source to prepare compositions with small oxygen content, because it is very stable against oxygen compared with metal Sr or metal nitride Sr_3N_2 [32]. Europium was added as the activator with the concentration of 2 at.% with respect to Sr atom. The Eu^{3+} ion in the starting powder Eu_2O_3 was reduced to Eu^{2+} under the nitrogen atmosphere during firing, which was confirmed by the absorption and emission spectra given later. The powder mixture was ground in the Si_3N_4 mortar and pestle. The mixed powder was filled in a hBN crucible and then fired in a graphite resistance furnace at 1900 °C for 6 h under 1 MPa nitrogen atmosphere. For comparison, Sr-SiAlON:Eu^{2+} [5/3] sample was also prepared using the same firing conditions. The starting composition of $Sr_{2.94}Eu_{0.06}Si_{12.75}Al_3O_{1.5}N_{21}$ was prepared from α-Si_3N_4: 35.25 mol %, SrO: 15.62 mol %, $SrSi_2$: 16.27 mol %, AlN: 32.54 mol %, and Eu_2O_3: 0.33 mol % (composition #2). Chemical compositions of synthesized Sr-SiAlON:Eu^{2+} samples were determined by the inductively coupled plasma-optical emission spectrometer (ICP-OES: IRIS Advantage, Nippon Jarrell-Ash, Yokohama, Japan) analysis for Sr, Eu, Si and Al, and inert gas fusion method (LECO: TC-436 St. Joseph, MI, USA) for O and N.

The formation of the [5/3] phase was confirmed by the profile fitting of X-ray diffractions for $10° \le 2\theta \le 120°$ with CuKα (Ultima III, Rigaku, Tokyo, Japan) at 0.01° intervals with a count time of 4 s per step. Using the structure data from a single crystal of $Sr_3Si_{15-x}Al_{1+x}O_xN_{23-x}$ ($x \approx 2$) [24], reliability factors $R_p = 0.0933$, $R_{wp} = 0.123$, $R_{all}(F) = 0.0365$, and $wR_{all}(F) = 0.0412$ were obtained. Refined cell parameters were $a = 14.7250(5)$ Å, $b = 9.0372(2)$ Å, $c = 7.4642(2)$ Å, and $\beta = 90.233(3)$. As shown in Table 1, the chemical analyze result confirmed the formation of [5/3] with the chemical composition of $Sr_{2.94}Eu_{0.06}Si_{13}Al_3O_2N_{21}$. The deviation of chemical compositions from the starting composition and the obtained Sr-SiAlON:Eu^{2+} [5/3] can be ascribed to the volatilization of some components of the starting composition at the high firing temperature of 1900 °C. The high-resolution diffraction data for the product with the starting composition of $Sr_{13.72}Eu_{0.28}Si_{60.2}Al_{12.32}O_{4.2}N_{99.4}$ were collected using a synchrotron radiation facility. The powder specimen was put into a quartz capillary tube with an inner diameter of 0.2 mm. The measurement was carried out with a wavelength of 0.65297 Å over a 2θ range up to 40° using a high-resolution diffractometer with Debye–Scherrer geometry installed at the BL15XU beamline in SPring-8 [33]. The phase identification was carried out by the profile fitting of diffraction data. Candidates of the phase were taken from the so-called Farey tree (Fig. 1), where possible commensurate phases $(AM_2X)_m(M_2X_4)_n$ in a range $8/5 \le n/m \le 5/3$ are systematically given. As a dimension of the *a*-axis of the $[n/m]$ phase is roughly given by $na_2 = 2.94n$ Å [26], the estimated value of *a* for [13/8], [18/11], [21/13], and [23/14] are 38.2, 52.9, 61.7, and 67.6 Å, respectively. The number of nonequivalent atoms in these phases is about 100 or more. The analysis for such long-period structures is difficult in a conventional manner. The (3+1)d superspace formalism [29–31] is used in our case, as the (3+1)d description has some advantages as follows. First, the number of possible peaks can be reduced considering the hierarchy of the main and satellite peaks in the earlier stage of the refinement. That is, satellite reflections of the higher order are eliminated from the list of possible peaks, and only main peaks and satellite peaks of the lower order (up to the 3rd order, for example) are considered for the indexing of observed peaks. As the present case is a composite crystal consisting of the two substructure, the indexing based on the (3+1)d description was performed imposing the condition that at least one of $|h_1|$ and $|h_2|$ is less than 4, for example. Second, a unified model in (3+1)d superspace, which was presented in our previous study [26], can be used as an initial model for any $[n/m]$ phases. The α ($=a_1/a_2$) component of the modulation wavevector should be set to the corresponding value of n/m, while fractional coordinates of atoms are unchanged. Third, the structure can be also treated as an incommensurate phase. Using the incommensurate option, the component of the modulation wavevector $\alpha = a_1/a_2$, which is the ratio of the cell dimensions for the two substructures, can be optimized in the refinement. This method is more efficient than comparing results from various commensurate phases to find which gives the best fitting. Programs used were JANA2006 [34] for calculations, and VESTA [35] for graphics.

The photoluminescence spectra of the powder samples were measured by the fluorescent spectrophotometer (Model F-4500, Hitachi Ltd., Japan) at room temperature with a 150 W Ushio xenon short arc lamp. The emission spectrum was corrected for the spectral response of a monochromator and Hamamatsu R928P photomultiplier tube by a light diffuser and tungsten lamp (Noma, 10 V, 4 A). The excitation spectrum was also corrected for the spectral distribution of the xenon lamp intensity by measuring rhodamine-B as reference. Temperature-dependent

Table 1
Chemical compositions of the obtained Sr-SiAlON:Eu^{2+}: (a) [23/14] and (b) [5/3].

	Composition						
	Sr	Eu	Si	Al	O	N	Total
(a)							
Weight %	24.9(1)	0.90(1)	35.4(1)	7.15(1)	2.37(4)	27.3(1)	98.02
Atomic %	7.26	0.15	32.21	6.77	3.79	49.81	
Atomic ratio[a]	13.71	0.29	60.83	12.79	7.15	94.06	
(b)							
Weight %	24.9(1)	0.94(1)	34.8(1)	8.16(1)	3.19(4)	27.1(1)	99.09
Atomic %	7.17	0.16	31.24	7.63	5.03	48.78	
Atomic ratio[a]	2.94	0.06	12.80	3.12	2.06	19.99	

[a] Modified to obtain suitable values for [23/14] or [5/3].

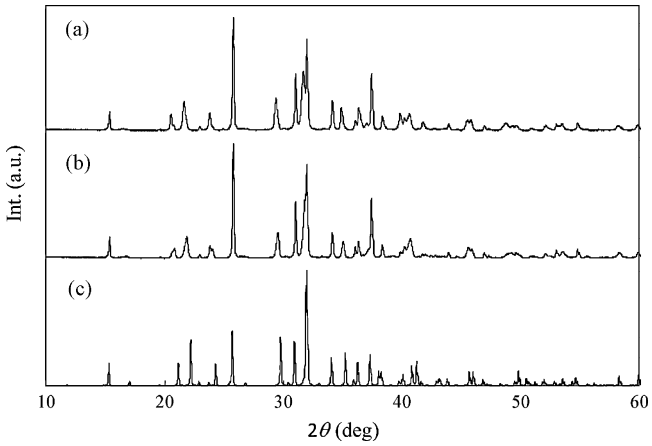

Fig. 2. X-ray powder diffraction patterns of products with the starting composition: (a) composition #2, (b) composition #1, and (c) simulated X-ray powder diffraction pattern of $Sr_5Si_{21}Al_5O_2N_{35}$ (ICSD #420168).

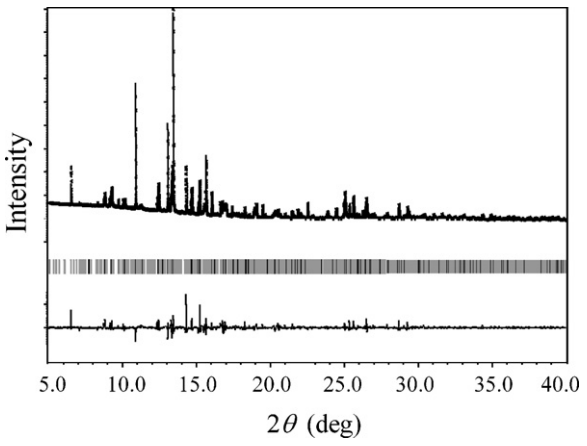

Fig. 3. Observed and calculated X-ray powder diffraction patterns for Si-SiAlON [23/14]. Solid line is the calculated pattern from the refined crystal structure. Residual errors are drawn at the bottom of the figure. Vertical short lines are allowed peak positions satisfying Bragg condition.

luminescence properties were recorded on an intensified multichannel spectrophotometer (MCPD-7000, Otsuka Electrics, Japan) with a 200 W Xe-lamp as an excitation source. The powder samples were heated from room temperature to 300 °C with a heating rate of 100 °C/min, and kept for 5 min for each temperature point.

3. Results and discussion

3.1. Structural characterization

The diffraction pattern of the product from composition #1 is basically similar to that of the [5/3] phase. However, the positions of some peaks significantly deviated from those of [5/3] or [8/5] phases (Fig. 2). Therefore, it is assumed that the obtained phase is one of the members in the composite crystal series $(AM_2X)_m(M_2X_4)_n$, but neither [5/3] nor [8/5]. The phase identification was carried out using the high-resolution diffraction data and the Farey tree as follows. A unified (3+1)d model given in the previous study [26] was used as an initial structure. A superspace group $P2_1(\alpha 0 \gamma)0$ was used considering the deviation of β from 90°. The cell parameters including the component α ($=a_1/a_2$) for the modulation wavevector were refined along with background and peak profile parameters. The refined a_1/a_2 ($=n/m$) ratio as an incommensurate structure was 1.641, which is close to a rational value 23/14 in the Farey tree (Fig. 1). Reliability factors from the refinement as a [23/14] commensurate structure were $R_p = 0.0203$, $R_{wp} = 0.0386$, $R_{all}(F) = 0.0633$, and $wR_{all}(F) = 0.0560$. Thus, it is concluded that the product is the [23/14] phase. The cell parameters are $a_1 = 4.8421(2)$ Å, $b = 9.0416(2)$ Å, $c = 7.4686(1)$ Å, $a_2 = 2.9474(1)$ ($=a_1 \times 14/23$) Å, and $\beta = 90.121(4)°$, which is converted to a superstructure in 3d space with a monoclinic cell of $a = 67.789(3)$ Å, $b = 9.0416(2)$ Å, $c = 7.4686(1)$ Å, and $\beta = 90.121(4)°$ of a space group $P2_1$ (Fig. 3).

After the refinement of cell parameters, structural parameters such as fractional coordinates were successively refined in the usual process of the profile fitting. In (3+1)d description, deviation of the initial structure model from the real one is corrected by Fourier coefficients. In the present case, however, it was impossible to refine these structure parameters. That is, the refined structures have unrealistic interatomic distances, or the Fourier coefficients cannot be successfully diverged in many cases. Nonetheless, the structure model used for the refinement of cell parameters seems fairly close to the real structure, judging from the reliability factors mentioned above. Additionally, the chemical analyze result reveals that the product is the [23/14] phase. As shown in Table 1, the atomic ratio is close to $Sr_{14}Si_{68-s}Al_{6+s}O_sN_{106-s}:Eu^{2+}$ ($s \approx 7$), indicative of the formation of [23/14] phase. The difference of chemical compositions between the starting composition and the obtained Sr-SiAlON:Eu^{2+} [23/14] is attributed to the volatilization of some components of the starting composition at the high firing temperature of 1900 °C, as mentioned above. The structural parameters converted to the superstructure in 3d space are provided as Supplementary data. A projection along the *a*-axis of the structure model for [23/14] is given in Fig. 4. As is common to all phases in this composite crystal series, two framework units are seen in the structure, which are projected along the *c*-axis in Fig. 5.

3.2. Dependence of photoluminescence properties of Sr-SiAlON:Eu^{2+} on the host lattice

Fig. 6 shows the excitation and emission spectra of (a) Sr-SiAlON:Eu^{2+} [23/14] and (b) Sr-SiAlON:Eu^{2+} [5/3] phosphors. The excitation spectrum of Sr-SiAlON:Eu^{2+} [23/14] phosphor covers the spectral region ranging from the UV to the visible light part. A broad excitation band is observed with a maximum at about 370 nm corresponding to the $4f^7 \rightarrow 4f^65d$ transition of Eu^{2+}. The emission spectrum shows a single intense broad emission band ranging from 400 nm to 700 nm, which is attributable to the allowed $4f^65d \rightarrow 4f^7$ transition of Eu^{2+}. The emission intensity of Sr-SiAlON:Eu^{2+} [23/14] phosphor is 92% of that of Sr-SiAlON:Eu^{2+} [5/3]. The characteristic Eu^{3+} luminescence which exhibits sharp and line spectrum between 560 nm and 630 nm was not observed. This suggests that

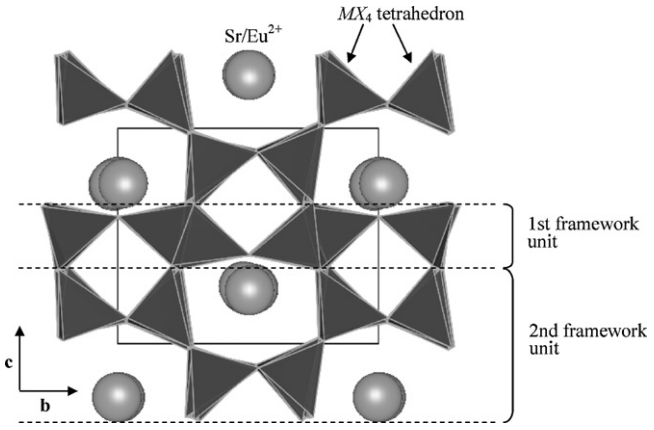

Fig. 4. A projection along the *a*-axis of the structure model for [23/14].

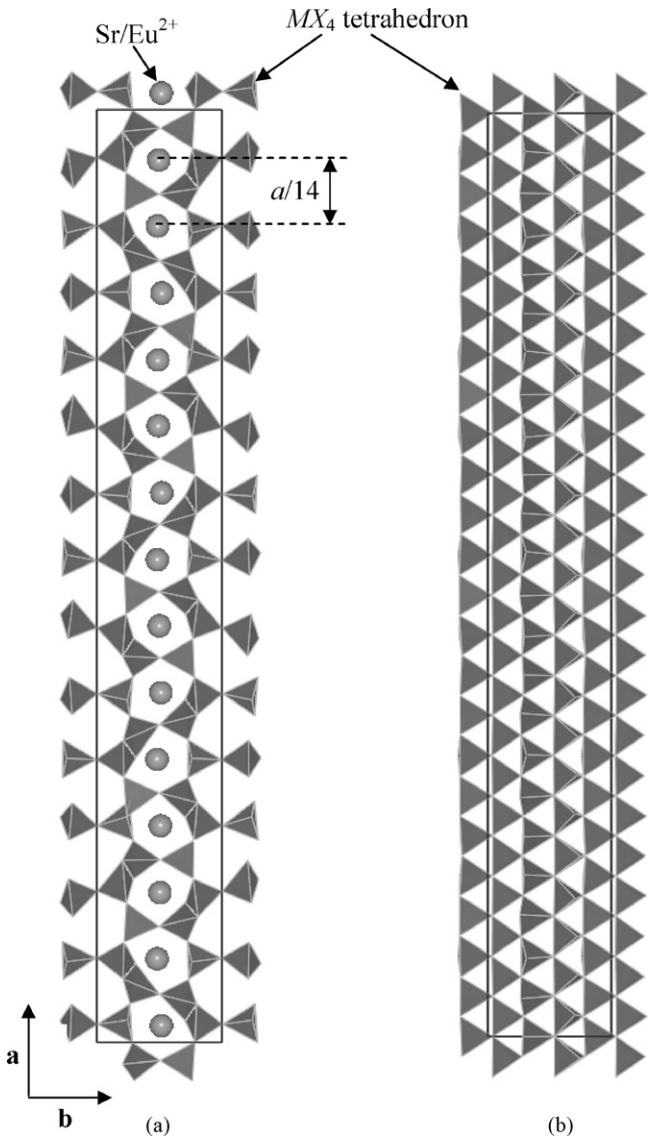

Fig. 5. Projection along *c*-axis of (a) the first framework unit and Sr/Eu^{2+} ions, and (b) the second framework unit in [23/14].

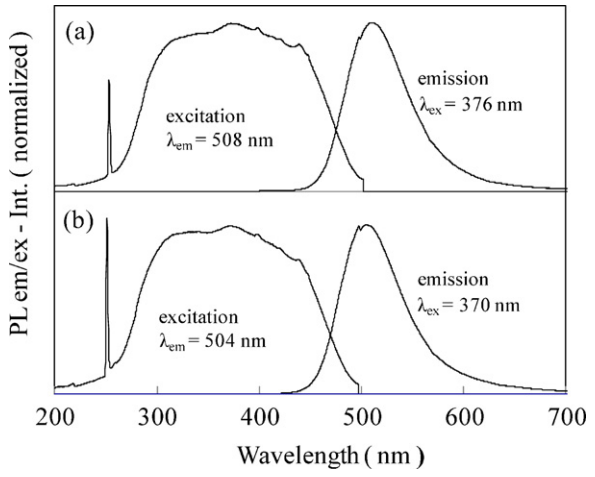

Fig. 6. Excitation and emission spectra of the samples: (a) [23/14], and (b) [5/3].

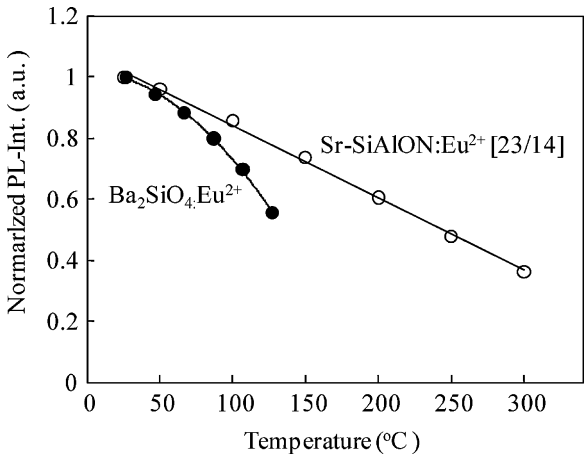

Fig. 7. Temperature dependence of PL intensity of [23/14] and $Ba_2SiO_4:Eu^{2+}$.

the europium ion in Sr-SiAlON phosphor is mainly in the divalent state. The overlap of the excitation and emission spectra is relatively small for the present Sr-SiAlON:Eu^{2+} [23/14] phosphor, suggesting that the re-absorption and/or energy transfer between the Eu^{2+} ions could be also small. The emission peak wavelength of Sr-SiAlON:Eu^{2+} [23/14] phosphor is about 508 nm, which is shorter than that of typical green emitting β-SiAlON:Eu^{2+} phosphor (535 nm). As a result, the use of the Sr-SiAlON:Eu^{2+} [23/14] phosphor can improve the color rendering index of white LEDs for general lighting when combined with a blue-LED and a β-SiAlON:Eu^{2+} phosphor as well as a red phosphor.

Meanwhile, the emission peak wavelength of Sr-SiAlON:Eu^{2+} [23/14] (508 nm) is slightly longer than that of Sr-SiAlON:Eu^{2+} [5/3] (504 nm). It is believed that the long wavelength emission of (oxy)nitride phosphors is attributed to covalent chemical bonding and a large crystal-field splitting effect on the Eu^{2+} 5d energy levels due to the presence of coordinating nitrogen [36]. Li et al. reported that $SrYSi_4N_7:Eu^{2+}$ has longer emission wavelength than that of $BaYSi_4N_7:Eu^{2+}$, and ascribed this to shorter metal–ligand distances in $SrYSi_4N_7:Eu^{2+}$ [37]. Similarly, the unit cell dimensions are $a = 67.789(3)$ Å, $b = 9.0416(2)$ Å and $c = 7.4686(1)$ Å for Sr-SiAlON:Eu^{2+} [24/13], and $a = 14.7250(5)$ Å, $b = 9.0372(2)$ Å, and $c = 7.4642(2)$ Å for Sr-SiAlON:Eu^{2+} [5/3]. Moreover, the basic period of the first substructure along the *a*-axis of Sr-SiAlON:Eu^{2+} [23/14] is smaller than that of Sr-SiAlON:Eu^{2+} [5/3]: $a/m = 4.842$ Å and 4.908 Å for Sr-SiAlON:Eu^{2+} [23/14] and Sr-SiAlON:Eu^{2+} [5/3], respectively. Meanwhile, the basic period of the 2nd substructure along the *a*-axis are $a/n = 2.947$ Å [23/14] and 2.945 Å [5/3]. The difference of the first substructure can be ascribed to the flexibility of the first substructure. Since the basic period of the first substructure a/m represents the size of AM_2X along the *a*-axis, the metal–ligand distances depend on a/m. It suggests that the longer emission wavelength can be ascribed to the larger crystal-field splitting resulting from the difference of a/m between Sr-SiAlON:Eu^{2+} [23/14] and Sr-SiAlON:Eu^{2+} [5/3]. Additionally, it seems that the emission wavelength can be controlled by varying a/m.

3.3. Thermal stability of Sr-SiAlON:Eu^{2+}

Fig. 7 shows the thermal stability of Sr-SiAlON:Eu^{2+} [23/14]. It is observed that the thermal stability of Sr-SiAlON:Eu^{2+} [23/14] is higher than that of typical blue-green emitting $Ba_2SiO_4:Eu^{2+}$ [21,22]. The residual emission intensity of Sr-SiAlON:Eu^{2+} [23/14] at 100 °C and 150 °C is still as high as 86% and 70%, respectively, of

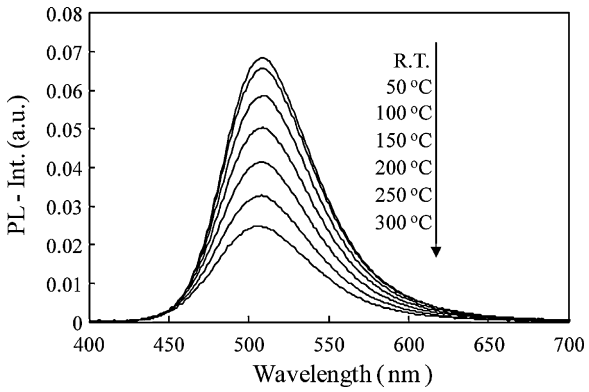

Fig. 8. Temperature dependence of emission spectra of [23/14].

the initial intensity at room temperature, whereas it is only 69% for $Ba_2SiO_4:Eu^{2+}$ (at 100 °C). As a result, Sr-SiAlON:Eu^{2+} [23/14] promises the improvement of the stability of color point of high-power white-LEDs when it is combined with other phosphors, such as green-, yellow-, and red-emitting phosphors. The results are almost comparable to the previous study [23]. According to Fukuda et al., the thermal stability of $Sr_3Si_{13}Al_3O_2N_{21}:Eu^{2+}$ is higher than that of $Ba_2SiO_4:Eu^{2+}$, and the difference of the thermal stability is mainly ascribed to the magnitude of electron–phonon interaction as a result of the difference of the host crystal structure, especially the connection of MX_4 tetrahedron, between $Sr_3Si_{13}Al_3O_2N_{21}:Eu^{2+}$ and $Ba_2SiO_4:Eu^{2+}$. As mentioned above, the crystal structure of Sr-SiAlON:Eu^{2+} [23/14] is similar to that of $Sr_3Si_{13}Al_3O_2N_{21}:Eu^{2+}$, which is largely different from the crystal structure of $Ba_2SiO_4:Eu^{2+}$. The crystal structure of Sr-SiAlON:Eu^{2+} [23/14] and $Sr_3Si_{13}Al_3O_2N_{21}:Eu^{2+}$ are constructed by the connection of MX_4 tetrahedra. In contrast, $Ba_2SiO_4:Eu^{2+}$ has no connection between MX_4 with isolated tetrahedra [38]. In this case, the host crystal structure of Sr-SiAlON:Eu^{2+} [23/14] can be maintained by the rigid framework with the connection of MX_4 tetrahedra at high temperature. It is believed that the rigid host lattice decreases the probability of the non-radiative transition, suggesting that the Stokes shift loss of Sr-SiAlON:Eu^{2+} [23/14] is smaller than that of $Ba_2SiO_4:Eu^{2+}$ at high temperature. As a result, Sr-SiAlON:Eu^{2+} [23/14] shows higher thermal stability than $Ba_2SiO_4:Eu^{2+}$. In addition, only very limited blue-shift of the emission band of Sr-SiAlON:Eu^{2+} [23/14] with increasing temperature was observed due to a high rigid host lattice. Furthermore, the blue-shift of the emission bands at high temperature is probably related to the thermal expansion or structural relaxation of the host lattice impacted on the 5d excitation levels of Eu^{2+} (see Fig. 8). These experimental results show that the Sr-SiAlON:Eu^{2+} [23/14] phosphor is a promising blue-green phosphor for creating white-light when combined with high-power blue-LED chips.

4. Conclusions

A novel Eu^{2+} activated Sr-SiAlON oxynitride phosphor, with the chemical formula of $Sr_{14}Si_{68-s}Al_{6+s}O_sN_{106-s}:Eu^{2+}$ ($s \approx 7$) was synthesized by firing the powder mixture of SrO, $SrSi_2$, α-Si_3N_4, AlN and Eu_2O_3 at 1900 °C for 6 h under 1 MPa nitrogen atmosphere. The structure was constructed by the connection of MX_4 tetrahedra (M: Si or Al; X: O or N), and Sr and Eu^{2+} ions as the guest ions. As the structure was considered to be two substructures comprising AM_2X for the first substructure and M_2X_4 for the second substructure, it is demonstrated that the structure is strongly associated with $Eu_3Si_{15-x}Al_{1+x}O_xN_{23-x}$ ($x \approx 5/3$) or $Sr_3Si_{15-x}Al_{1+x}O_xN_{23-x}:Eu^{2+}$ ($x \approx 2$) and $Sr_5Si_{21-x}Al_{5+x}O_{2+x}N_{35-x}:Eu^{2+}$ ($x \approx 0$). The chemical formula of synthesized Sr-SiAlON:Eu^{2+} for a whole crystal has been given by $(AM_2X)_m(M_2X_4)_n$ ($[n/m] = [23/14]$), which is one of the phases between [8/5] and [5/3]. The Sr-SiAlON:Eu^{2+} [23/14] shows the excitation wavelength ranging from the ultraviolet region to 500 nm, and exhibits an intense blue-green light due to the $4f^65d \rightarrow 4f^7$ transition of Eu^{2+}. Given a rigid lattice, the thermal stability of blue-green emitting Sr-SiAlON:Eu^{2+} [23/14] is relatively high and its residual emission intensity of Sr-SiAlON:Eu^{2+} [23/14] at 150 °C is 70% of the initial intensity at room temperature. It shows that the Sr-SiAlON:Eu^{2+} [23/14] is a promising blue-green phosphor for creating white-light when combined with high-power blue-LED chips.

Acknowledgement

The authors would like to thank Mr. Yoshiyuki Yajima from the NIMS (Tsukuba) for the chemical analysis.

Appendix A. Supplementary data

Supplementary data associated with this article can be found, in the online version, at doi:10.1016/j.jallcom.2010.09.021.

References

[1] S. Nakamura, G. Fasol, The Blue Laser Diode: GaN Based Light Emitters and Lasers, Springer-Verlag, Berlin, 1997.
[2] Y. Sato, N. Takahashi, S. Sato, Jpn. J. Appl. Phys. 35 (1996) 838–839.
[3] Y. Narukawa, I. Niki, K. Izuno, M. Yamada, Y. Murazaki, T. Mukai, Jpn. J. Appl. Phys. 41 (2002) 371–373.
[4] Y.D. Huh, J.H. Shim, Y. Kim, Y.R. Do, J. Electrochem. Soc. 150 (2003) H57–H60.
[5] H.A. Hoppe, H. Lutz, P. Morys, W. Schnick, A. Seilmeier, J. Phys. Chem. Solids 61 (2000) 2001–2006.
[6] Y.Q. Li, J.E.J. van Steen, J.W.H. van Krevel, G. Botty, A.C.A. Delsing, F.J. DiSalvo, G. de With, H.T. Hintzen, J. Alloys Compd. 417 (2006) 273–279.
[7] K. Uheda, N. Hirosaki, Y. Yamamoto, A. Naito, T. Nakajima, H. Yamamoto, Electrochem. Solid State Lett. 9 (2006) H22–H25.
[8] K. Uheda, N. Hirosaki, H. Yamamoto, Phys. Status. Solid A 203 (2006) 2712–2717.
[9] H. Watanabe, N. Kijima, J. Alloys Compd. 475 (2009) 434.
[10] C. Hecht, F. Stadler, P.J. Schmidt, J.S. auf der Günne, V. Baumann, W. Schnick, Chem. Mater. 21 (2009) 1595.
[11] J.W.H. van Krevel, J.W.T. van Rutten, H. Mandal, H.T. Hintzen, R. Metselaar, J. Solid State Chem. 165 (2002) 19–24.
[12] R.-J. Xie, M. Mitomo, K. Uheda, F.-F. Xu, Y. Akimune, J. Am. Ceram. Soc. 85 (2002) 1229–1234.
[13] R.-J. Xie, N. Hirosaki, K. Sakuma, Y. Yamamoto, M. Mitomo, Appl. Phys. Lett. 84 (2004) 5404–5406.
[14] R.-J. Xie, N. Hirosaki, M. Mitomo, Y. Yamamoto, T. Suehiro, K. Sakuma, J. Phys. Chem. B 108 (2004) 12027–12031.
[15] J.A. Kechele, C. Hecht, O. Oeckler, J.S. Günne, P.J. Schmidt, W. Schnick, Chem. Mater. 21 (2009) 1288–1295.
[16] J.W.H. van Krevel, H.T. Hintzen, R. Metselaar, A. Meijerink, J. Alloys Compd. 268 (1998) 272–277.
[17] N. Hirosaki, R.-J. Xie, K. Kimoto, T. Sekiguchi, Y. Yamamoto, T. Suehiro, M. Mitomo, Appl. Phys. Lett. 86 (2005) 211905.
[18] Y.Q. Li, A.C.A. Delsing, R. Metslaar, G. de With, H.T. Hintzen, J. Alloys Compd. 487 (2009) 28–33.
[19] R.-J. Xie, N. Hirosaki, Y.Q. Li, T. Takeda, J. Lumin. 130 (2010) 266–269.
[20] Y.Q. Li, N. Hirosaki, R.-J. Xie, T. Takeda, M. Mitomo, J. Lumin. 130 (2010) 1147–1153.
[21] T.L. Barry, J. Electrochem. Soc. 115 (1968) 1181–1184.
[22] J.S. Kim, Y.H. Park, S.M. Kim, J.C. Choi, H.L. Park, Solid State Commun. 133 (2005) 445–448.
[23] Y. Fukuda, K. Ishida, I. Mitsuishi, S. Nunoue, Appl. Phys. Express 2 (2009) 012401–012403.
[24] N. Ishizawa, M. Kamoshita, K. Fukuda, K. Shioi, N. Hirosaki, Acta Crystallogr. E66 (2010) i14.
[25] O. Oeckler, J.A. Kechele, H. Koss, P.J. Schmidt, W. Schnick, Chem. Eur. J. 15 (2009) 5311–5319.
[26] Y. Michiue, K. Shioi, N. Hirosaki, T. Takeda, R.-J. Xie, A. Sato, M. Onoda, Y. Matsushita, Acta Crystallogr. B65 (2009) 567–575.
[27] A. Yamamoto, Acta Crystallogr. A52 (1996) 509–560.
[28] S. van Smaalen, Incommensurate Crystallography, Oxford University Press, New York, 2007.
[29] P.M. de Wolff, Acta Crystallogr. A30 (1974) 777–785.
[30] A. Janner, T. Janssen, Acta Crystallogr. A36 (1980) 399–408.
[31] A. Janner, T. Janssen, Acta Crystallogr. A36 (1980) 408–415.

[32] K. Shioi, N. Hirosaki, R.-J. Xie, T. Takeda, Y.Q. Li, J. Mater. Sci. 43 (2008) 5659–5661.
[33] M. Tanaka, Y. Katsuya, A. Yamamoto, Rev. Sci. Instrum. 79 (2008) 075106–075111.
[34] V. Petricek, M. Dusek, L. Palatinus, JANA2006, Structure Determination Software Programs, Institute of Physics, Praha, Czech Republic, 2006.
[35] K. Momma, F. Izumi, J. Appl. Crystallogr. 41 (2008) 653–658.
[36] J.W.H. van Krevel, Ph.D. Thesis, Eindhoven University of Technology, 2000.
[37] Y.Q. Li, C.M. Fang, G. de With, H.T. Hintzen, J. Solid State Chem. 177 (2004) 4687–4694.
[38] B. Michele, G. Gazzoni, G. Ivaldi, G. Zanini, Acta Crystallogr. B39 (1983) 674–679.